

InGaAs/InP Negative Feedback Avalanche Diodes (NFADs)

Xudong Jiang*, Mark A. Itzler, Kevin O'Donnell, Mark Entwistle, Krystyna Slomkowski
Princeton Lightwave Inc., 2555 US Route 130, Cranbury, NJ USA 08512

ABSTRACT

In recent years substantial effort has been made in material growth, device design and fabrication, and driving circuitry to improve the performance of InGaAs/InP single photon avalanche diodes (SPADs) operated in Geiger mode. Despite these efforts, InGaAs/InP SPADs are constrained by certain performance limitations due to the inherent positive feedback involved in the avalanche process. With the goal of overcoming some of these performance limitations, we have successfully designed and implemented thin film resistors monolithically integrated with InGaAs/InP SPADs to provide a negative feedback mechanism to regulate the avalanche sizes. The monolithic integration scheme ensures very small parasitic effects, results in fast quenching of avalanches, and allows for wafer-level integration which facilitates the fabrication of array structures. We will discuss the design and operation of NFAD devices and performance characterization of these devices. Basic characteristics of NFADs such as pulse response, quenching and recovery dynamics will be described. We will also present device performance parameters such as photon detection efficiency (PDE), dark count rate (DCR) and afterpulsing probability (P_{ap}). InGaAs/InP negative feedback avalanche diodes with different device sizes and quenching resistances have been designed and fabricated. Devices with $\sim 10\%$ PDE and acceptable P_{ap} has been realized, which provides a simple, practical solution for certain photon-counting applications.

Keywords: Avalanche photodiodes, single photon detector, SPAD, InGaAsP, negative feedback

1. INTRODUCTION

Single photon avalanche diodes (SPADs) operate in Geiger mode, in which biasing above the breakdown voltage accompanied by photoexcitation of just a single charge carrier can lead to a self-sustaining avalanche to produce a macroscopic current pulse that can be sensed using an appropriate threshold detection circuit. InP-based SPADs have high detection efficiency, low dark count rate, and low timing jitter at short-wave infrared (SWIR) wavelengths between 1.0 and 1.7 μm . Due to their good performance, compactness, high reliability, and low cost, these devices often provide the most practical solution for photon counting and photon timing applications at SWIR wavelengths. InP-based SPADs have found a wide range of applications in many diversified fields, such as optical time domain reflectometry [1], quantum cryptography [2], photon-correlation spectroscopy [3], fundamental studies in quantum physics [4], semiconductor devices and material characterization [5], laser ranging [6], biological imaging [7], as well as free space optical communications in photon-starved environments [8]. Over the past decade, a great effort has been made towards further improving the performance of InP SPADs and significant progress has been achieved [9].

A major shortcoming of regular SPADs is the positive feedback inherent in their avalanche dynamics and the associated performance degradation. With typical circuit implementations, the number of carriers involved in the avalanche of a typical SPAD is large ($\sim 10^7 - 10^8$). Even though significant progress has been made in improving the performance of InP SPADs, certain limitations remain. For example, the counting rate of these devices has often been limited to less than 10 MHz due to afterpulsing, and they do not have the ability to resolve photon number. These limitations constraint their use in many photon counting applications.

Negative feedback avalanche diodes (NFADs) could possibly resolve the two drawbacks of InP-based SPADs. In NFADs, a thin film quenching resistor with appropriate resistance is monolithically integrated with a SPAD. When an avalanche is triggered by either a photocarrier or dark carrier, the monolithically integrated resistor will quickly quench the avalanche and while also regulating the charge flow through the device. With NFADs we have fabricated to date, the number of carriers in an avalanche is reduced to the order of $10^5 - 10^6$, and further reduction is possible. The fast quenching and reduced charge flow inside the NFAD structure could significantly reduce the afterpulsing effect and therefore allow for increased photon counting rate.

*xjiang@princetonlightwave.com; tel: 1 609 495-2584; www.princetonlightwave.com

The concept of negative feedback was initially applied to detectors used in nuclear and particle physics experiment [10,11], where various resistors were monolithically integrated onto silicon APDs. This negative feedback concept has also been applied to InP-based SPAD by employing an epitaxial heterobarrier to quench avalanches [12]. Passive quenching achieved by hybrid integration of a quench resistor to a SPAD [13] often suffers from large parasitic effects [13,14] that degrades the device performance. Itzler *et al.* reported the first InP NFADs based on SPADs with monolithically integrated thin film resistors [15]. The NFADs avoid the large parasitic effects involved in typical hybrid passive quenching approaches and show evidence of phenomena that may be distinct from simple passive quenching.

In this paper, we describe the design and characterization of InP-based NFADs. In section 2 we present the design of the NFAD device and describe methods for their characterization. The characterization results are presented in section 3. Section 4 contains additional discussions of InP-based NFAD performance and concludes with a summary.

2. NFAD DESIGN AND METHOD OF CHARACTERIZATION

During the past few years, we have extended significant effort in the design and fabrication of high performance SPADs at both 1.06 μm and 1.55 μm [16–18]. This work on SPADs has laid a good foundation for making high performance NFADs. Figure 1 shows the experimentally measured dark count rate (DCR) versus photon detection efficiency (PDE) performance for eleven 1550 nm SPADs fabricated in the same process lot. The active area diameter is 25 μm for these devices, and the measurement was performed at 215 K. As can be seen from this figure, the best devices can achieve < 1 kHz DCR at PDE $> 20\%$.

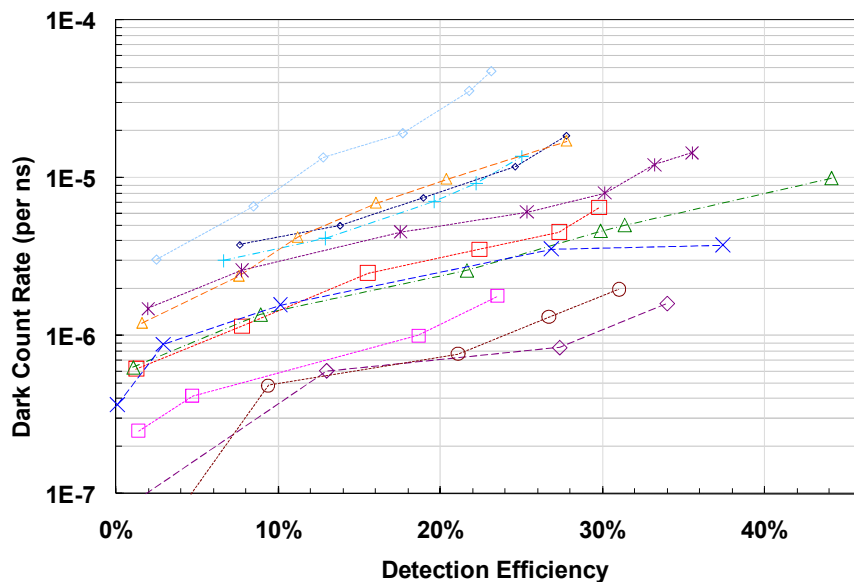


Figure 1. Measured dark count rate (DCR) versus photon detection efficiency (PDE) for eleven 1550 nm SPADs with active region diameter of 25 μm . The measurement was performed at 215 K.

In Figure 2, we provide a schematic illustration of our test set for characterizing NFADs. The NFAD is biased above the breakdown voltage by a Source-Measure Unit (SMU) through a bias tee. Avalanche pulses generated inside the NFAD are fed to an amplifier, and the output of the amplifier is connected to a Tektronix digital scope or a Signatec acquisition card. The digital scope has high resolution, but its depth of memory is limited. The Signatec PDA1000 card provides deep memory for capturing analog signal data with 1 ns resolution with data collection periods as long as 250 ms. We have also integrated a 1550 nm pulsed laser source (idQuantique id300) into this setup for making calibrated pulsed PDE measurements. Measurement timing is determined using an SRS DG535 pattern generator. Statistical information is extracted from a collection of 10,000 laser pulse repetitions. The repetition rate for the laser pulse is 50 kHz and the mean photon number per pulse is $\mu = 1$. The PDE can be extracted by summing the number of counts occurring at the photon arrival time. (Poisson corrections for $\mu = 1$ have been added.) The DCR was measured in the absence of illumination with a time duration of about 0.1 second. (Note that this DCR value includes afterpulses due to dark counts.)

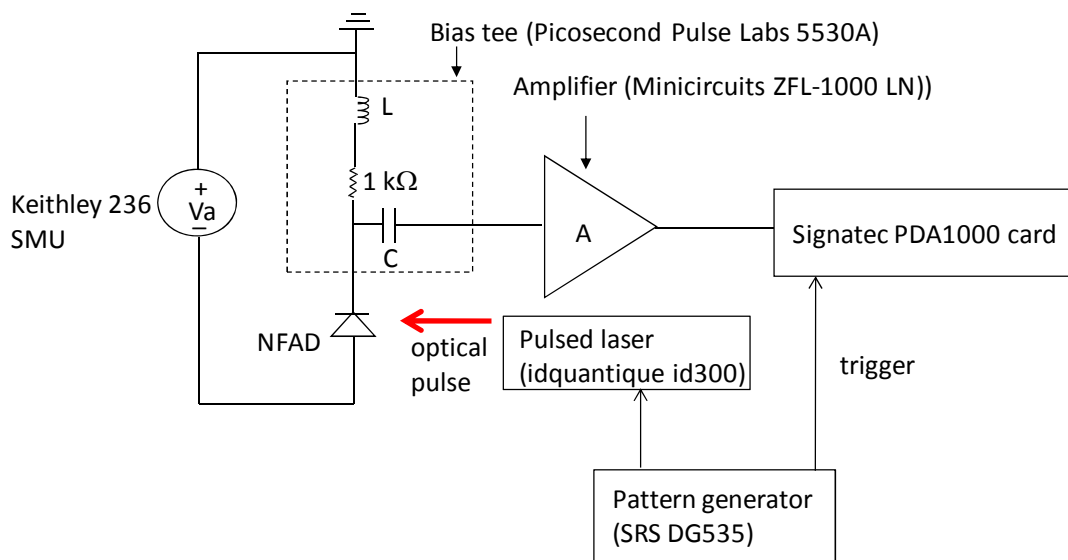


Figure 2. Schematic of test set-up for NFAD device characterization.

Resistances obtained from a first iteration of NFAD devices range from 25 to 110 k Ω , depending on the device size; and for a second iteration of NFADs, resistances are in the range of \sim 500 – 2800 k Ω [19]. Devices from the two iterations show distinct differences in their performances. Devices from the first iteration exhibit “persistent current”, i.e., with sufficient high bias voltages, the avalanche pulse response shows a very long (\sim 100 ns) period of persistent current flow before spontaneous quenching happens [19–21]. While this persistent current state is an interesting physical phenomenon, it adversely affects the device operation. The persistent current issue is absent in the second iteration devices. In the following sections, we will focus on results obtained from these second iteration devices. Table 1 lists the active area diameter and integrated resistor value for some of the devices fabricated in the second iteration.

Table 1. Active area diameter and integrated resistance for devices fabricated in second iteration.

Device	Active area diameter (μm)	Integrated resistance (k Ω)
E1G5	22	560
E3G3	32	740
E2G6	22	990
E4G4	42	1750
E3G7	32	1790

3. CHARACTERIZATION OF NFAD DEVICES

3.1 NFAD avalanche pulses

Figure 3 shows a typical avalanche pulse from device type E1G5 at \sim 1.5 V excess bias voltage and $T = 235$ K. When a dark carrier or photo-carrier triggers an avalanche, the avalanche current builds up quickly and shows up as a negative-going sharp peak in Figure 3. Given a fixed DC bias voltage across the NFAD device, as the avalanche current builds up in amplitude, the resulting voltage drop across the integrated resistor gradually shifts bias voltage away from the avalanche diode portion of the structure. With sufficient reduction of bias voltage (and associated current flow) in the avalanche diode, it will no longer support a self-sustaining avalanche, and the avalanche quenches. The current pulse obtained from the measurement apparatus exhibits a very narrow peak with full width at half maximum (FWHM) < 2 ns. Although the rise time is clearly sub-ns (see Figure 3), the 1-ns resolution of the Signatec data acquisition board does not allow a more precise determination of the rise time. The fall time is equally abrupt, although there is generally an additional short low-amplitude tail on the falling edge of the pulse. Other devices show similar behavior.

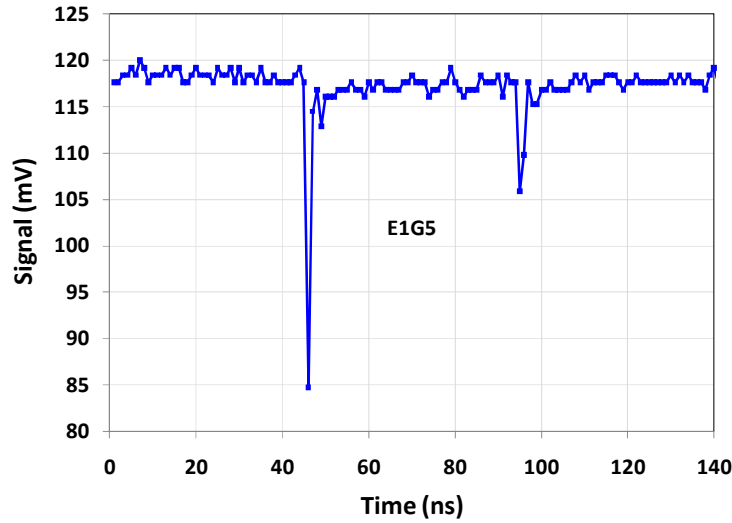


Figure 3. Avalanche pulses of NFAD device type E1G5 at ~ 1.5 V excess bias voltage and 235 K.

3.2 Avalanche statistics

To assess the reproducibility of the avalanche response to photon detections, we have determined the total avalanche charge flow per avalanche by integrating over each pulse response. While carrying out this analysis, we have used only detection events that corresponded to photon arrivals. Figure 4 shows the integrated avalanche charge as a function of excess bias voltage (red diamonds, left axis) for device E1G5 illuminated with photon pulses with a mean photon number per pulse of $\mu = 1$. When the excess bias voltage increases from 0.2 V to 1.6 V, the avalanche charge increases from $2.0 \times 10^5 e^-$ to $4.2 \times 10^5 e^-$.

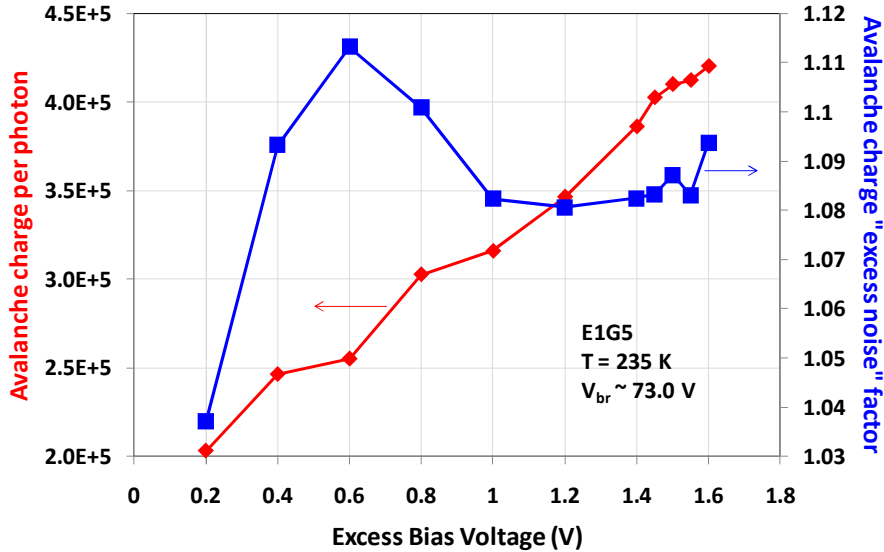


Figure 4. Measured avalanche charge per photon as a function of excess bias (red diamonds, left-hand axis) determined by integrating over pulse responses to incident photons. Variations in the avalanche charge is quantified by the “excess noise” F (blue squares, right-hand axis).

To reflect the variation in avalanche charge, a charge “excess noise” factor can be defined as $F(Q) = 1 + \sigma^2 / \langle Q \rangle^2$, where $\langle Q \rangle$ is the average integrated charge and σ is the standard deviation of the distribution of Q . The dependence of $F(Q)$ on excess bias voltage is also shown in Figure 4 (blue squares, right-hand axis). For excess bias voltage around 1 V, the excess noise factor is in the range of 1.07 – 1.09.

3.3 Afterpulsing probability

Figure 5 shows the dependence of afterpulsing probability P_{ap} on PDE for various NFAD devices, for measurements carried out at 236 K. Among these devices, E1G5 has much higher P_{ap} than other devices at any particular PDE. The reason may be due to the fact that E1G5 has the shortest recovery time, and therefore has a higher probability to trigger afterpulses at any given time period compared to other devices under the same PDE. At any given PDE, E4G4 has higher P_{ap} than E3G3, E2G6 and E3G7. E4G4 has the largest area, and for a given set of operating conditions, there may be more trapped carriers inside the multiplication region than there are for other type of devices. It should be noted that an afterpulsing probability of greater than 1 corresponds to situations in which initial afterpulses cause additional afterpulses, and so the net number of afterpulses per detected photon can be larger than 1. For devices other than E1G5, this “cumulative” afterpulsing probability remains less than 1 for PDE values up to about 10%.

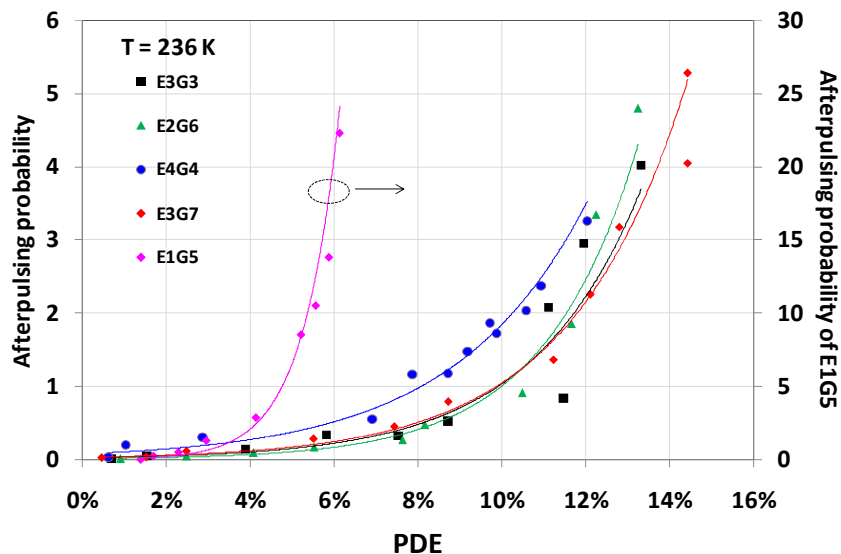


Figure 5. Dependence of afterpulsing probability on PDE for various NFAD device types at 236 K. The symbols are measured results and the lines are exponential fits to the experimental data.

From an application point of view, it is relevant to identify the maximum PDE that can be achieved at a particular P_{ap} level. Figure 6 shows the PDE that various devices can achieve under 50% and 100% P_{ap} .

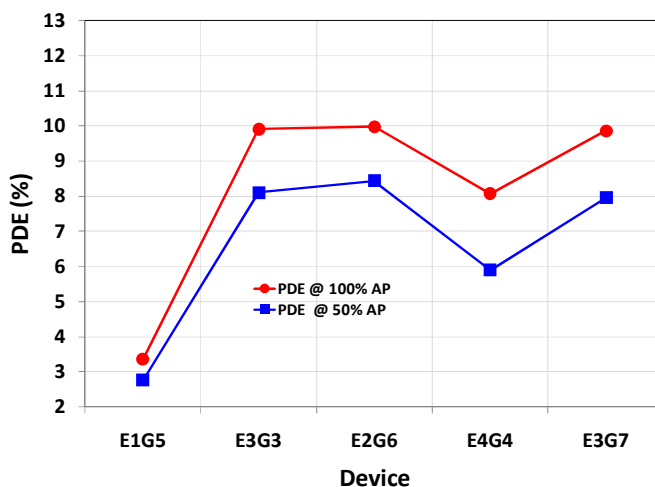


Figure 6. PDE at P_{ap} values of 50% and 100% for various NFAD devices at 236 K.

3.4 Timing jitter

Timing jitter refers to the variation in the correlation between the time of photon arrival and the time of the detection of the consequent avalanche pulse. Various mechanisms contribute to the timing jitter, such as (i) differences in the transit times of photoexcited carriers resulting from differences in the location of the photon absorption; (ii) carrier propagation delay caused by the temporary trapping of carriers at heterointerface formed by dissimilar semiconductor layers; and (iii) variations in the avalanche build-up time induced by the stochasticity of the impact ionization process. Among these different mechanisms, variation in avalanche build-up time is the principal contribution.

A simple Monte Carlo technique [22] can be used to model the contribution of avalanche build-up time variation to timing jitter. The random ionization path length of an electron x_e is described by the probability density function $h_e(x_e)$:

$$h_e(x_e) = \begin{cases} 0 & x_e \leq d_e \\ \alpha^* \exp[-\alpha^*(x_e - d_e)] & x_e > d_e \end{cases} \quad (1)$$

Where d_e is the electron dead space (within which no impact ionization event can occur) and α^* is the “enabled” electron ionization coefficient. The electron survival probability is then

$$S_e(x_e) = \int_0^{x_e} h_e(x) dx = \begin{cases} 1 & x_e \leq d_e \\ \exp[-\alpha^*(x_e - d_e)] & x_e > d_e \end{cases} \quad (2)$$

By substituting a uniformly distributed random number r between 0 and 1 for $S_e(x_e)$, the electron random ionization path length can be obtained as

$$d_e = x_e - \frac{\ln(r)}{\alpha^*} \quad (3)$$

Similar expressions can be defined for the hole ionization path length, and at any given time t , the current $I(t)$ is

$$I(t) = \frac{q}{W} [N(t)v_{se} + P(t)v_{sh}] \quad (4)$$

where q is the electron charge, W is the multiplication region width. $N(t)$ and $P(t)$ are the number of electrons and holes inside the multiplication region at time t , respectively. v_{se} and v_{sh} are the electron and hole saturation velocity, respectively.

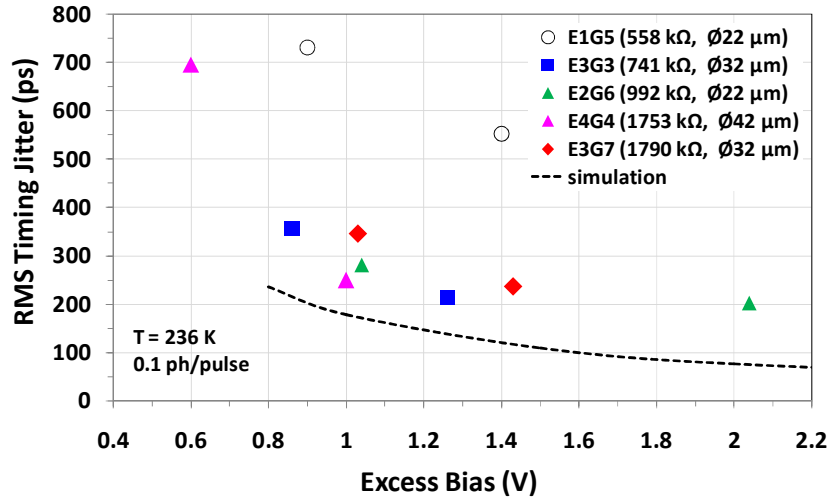


Figure 7. RMS jitter for NFAD devices under different excess bias voltages at $T = 236$ K and 0.1 photon/pulse. Symbols are measured results and the solid line is the simulated result.

By choosing a suitable threshold current, the timing jitter can be calculated from (1)–(4). We have characterized the timing jitter of various NFAD devices by recording the avalanche trace on the digital scope with a resolution of 100 ps, and then find the variation of time crossing a particular threshold level (10 mV). Figure 7 shows the extracted RMS jitter

for different NFAD devices along with the timing jitter simulated using (1)–(4). The general trend between the measured result and the simulation is similar, although the simulated result is ~ 100 ps lower than the measurements in the excess bias range of 1 – 2 V. We note that we have not attempted to subtract any system-level jitter from the measurement data, and this is likely to be significant.

3.5 Dark count performance and device recovery characteristics

We have also characterized the dark count performance of these NFAD devices. The pulse height of the second peak (V_{2amp}) of consecutive avalanche pulse pairs versus the inter-arrival time (ΔT) between these two pulses can be constructed from the dark count measurement, and this provides important information on the device recovery characteristics.

Figure 8(a) shows the measured V_{2amp} vs. ΔT for E1G5 at 235 K at 1.4 V excess bias voltage, along with the moving average of the measured data. Figure 8(b) shows the exponential fitting to the moving average, from which the recovery time constant can be extracted. The extracted recovery time is 55 ns, in good agreement with 46 ns which is estimated from the device resistance and capacitance.

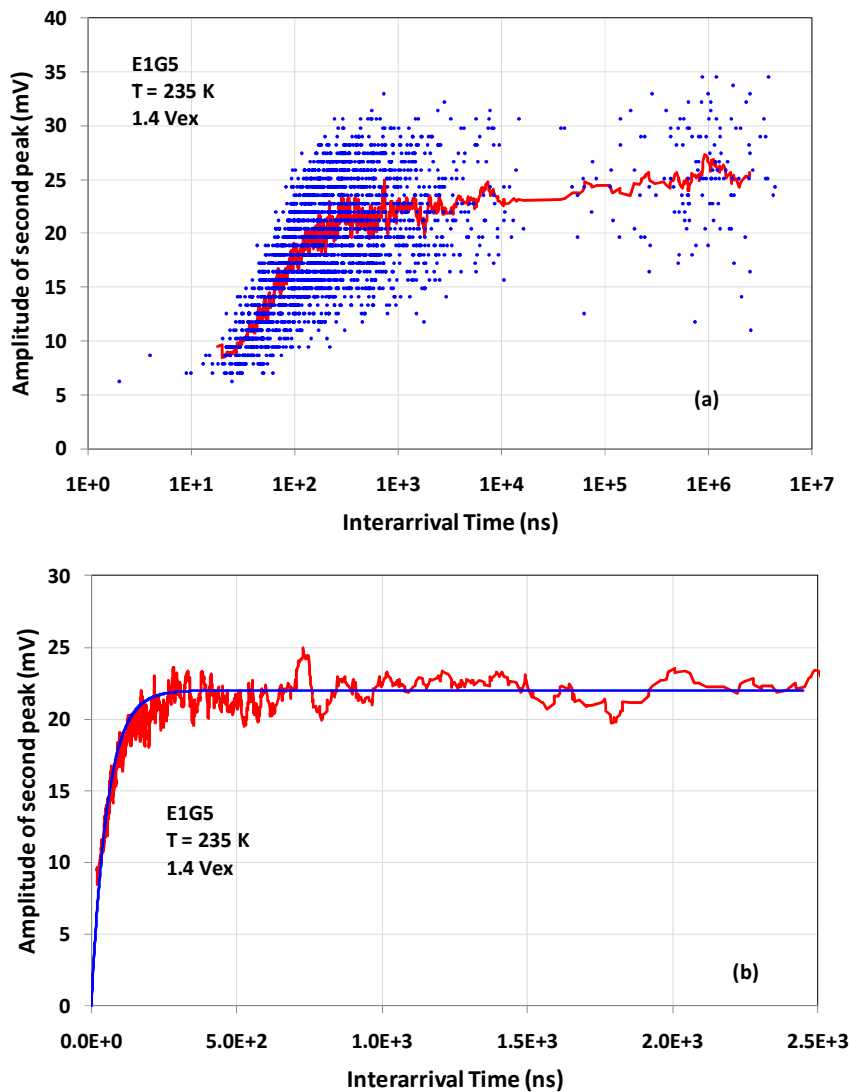


Figure 8. Dependence of second peak height V_{2amp} of consecutive avalanche pulse pairs on inter-arrival time ΔT (a) and the exponential fitting to the $V_{2amp} - \Delta T$ curve (b). Blue dots are measured results, red line is the moving average of the measured data, and solid blue line is the exponential fitting to the moving average.

4. DISCUSSIONS AND CONCLUSIONS

We have fabricated and characterized NFAD devices with different active region sizes and monolithically integrated resistors. The integrated resistor greatly reduces the charge flow and parasitic capacitance, and as a result of this the number of carriers involved in an avalanche is significantly smaller than that of typical gated or actively quenched SPAD implementations as well as hybridly integrated passive-quenching SPADs. This reduced current flow can significantly reduce afterpulsing probability at any given PDE and may create opportunities for SPAD in new applications, especially those applications which require free running operation. The integrated resistor also regulates the avalanche size so that the avalanche pulses have a low charge “excess noise” factor, which provides the possibility of resolving photon number when putting the NFAD devices into a matrix format.

Afterpulsing remains a challenge for NFAD devices operated in free running mode even with significantly reduced avalanche charge flow. We point out that this issue is not isolated to InP-based devices: even in Si self-quenching devices based on the monolithic integration of polysilicon resistors, afterpulsing remains a significant effect, with afterpulsing probabilities of at least ~20–40% for 10% PDE [23]. A fundamental solution for reducing afterpulsing probability would be to further improve material quality and get rid of—or at least greatly reduce—the number of traps responsible for afterpulsing. As has been shown in section 3.3, the afterpulsing probability also has some dependence on device parameters and can be further improved by optimizing device parameters. In particular, we believe we can reduce current flow—and presumably, the associated afterpulsing—by at least another factor of 10 and still have readily detectable avalanche signals.

Our initial study of the timing jitter performance of NFAD devices show that most devices can achieve 200 – 250 ps RMS jitter at 1–2 V excess bias voltage. Our simulation reveals that variation in avalanche build-up time is the principal contribution to timing jitter. Avalanche build-up time depends sensitively on avalanche multiplication width, and a narrower multiplication region width will improve device timing jitter performance. On the other hand, a narrower multiplication region width will also lead to somewhat higher dark count rate due to trap-assisted tunneling effects in narrower avalanche regions with higher breakdown electric fields. Depending on the specific application requirements, an optimized design may be realized by carefully taking into account the dependence of timing jitter and dark count rate on multiplication region width.

Our work on InP-based NFAD devices has shown that devices with good PDE and acceptable afterpulsing probability can be achieved, and this provides a simple, practical solution in certain photon counting applications. With further understanding of the device performance, improved device design, and more effort on material growth, we expect to obtain InP-based NFAD devices with even higher performance. This will open doors to a wider range of applications which require single photon sensitivity in the SWIR spectral range with simple detector operation (e.g., free running mode).

REFERENCES

1. B. F. Levine, C. G. Bethea and J. C. Campbell, “Room temperature 1.3- μm optical time reflectometer using a photon counting InGaAs/InP avalanche detector”, *Appl. Phys. Lett.* **46**(4), 333-335 (1985).
2. N. Gisin, G. Ribordy, W. Tittel and H. Zbinden, “Quantum cryptography”, *Rev. Mod. Phys.* **74**(1), 145-195 (2002).
3. R. G. W. Brown, K. D. Ridley and J. G. Rarity, “Characterization of silicon avalanche photodiodes for photon-correlation measurements. I: Passive quenching”, *Appl. Opt.* **25**(22), 4122–4126 (1986).
4. J. G. Rarity and P. R. Tapster, “Experimental violation of Bell’s inequality based on phase and momentum”, *Phys. Rev. Lett.* **64**(21), 2495-2498 (1990).
5. A. L. Lacaita, F. Zappa, S. Bigliardi and M. Manfredi, “On the bremsstrahlung origin of hot-carrier-induced photons in silicon devices”, *IEEE Trans. Electron Devices* **40**(3) 57-82 (1993).
6. R. M. Measures, *Laser Remote Sensing – Fundamentals and Applications*, John Wiley & Sons, 1984.
7. K. Suhling, J. Siegel, D. Phillips, P.M.W. French, S. L  v  que-Fort, S.E.D. Webb and D. M. Davis, “Imaging the environment of green fluorescent protein”, *Biophysical Journal* **83** (6), 3589-3595 (2002).
8. Special issue on “Free-space communication techniques for optical networks”, *IEEE LEOS Newsletter* **19** (5), 6-39 (2005).
9. M. A. Itzler, X. Jiang, M. Entwistle, K. Slomkowski, M. Owens, A. Tosi, F. Acerbi, F. Zappa, and S. Cova, “Advances in InGaAsP-based avalanche diode single photon detectors,” *J. Modern Optics* **58**, 174 – 200 (2011).
10. V. E. Shubin and D. A. Shushakov, “New avalanche device with the ability of analog few-photon pulse detection”, *Proceedings of the SPIE* **2550**, 284 – 293 (1995).

11. D. Bisello, Yu. Gotra, V. Jejcerc, V. Kushpil, N. Malakhov, A. Paccagnella, Z. Sadygov I. Stavitsky and E. Tsyganov, "Silicon avalanche detectors with negative feedback for high energy physics", *Nuclear Instruments and Methods in Physics Research A* **367**, 212 – 214 (1995).
12. K. Zhao, A. Zhang, Y.-h. Lo and W. Farr, "InGaAs single photon avalanche detector with ultralow excess noise", *Appl. Phys. Lett.* **91**(8), 081107 (2007).
13. S. Cova, M. Ghioni, A. Lacaita, C. Samori and F. Zappa, "Avalanche photodiodes and quenching circuits for single-photon detection", *Appl. Opt.* **35**(12), 1956–1976 (1996).
14. R.E. Warburton, M. Itzler and G.S. Buller, "Free-running, room temperature operation of an InGaAs/InP single-photon avalanche diode", *Appl. Phys. Lett.* **94**, 071116 (2009).
15. M. A. Itzler, X. Jiang, B. Nyman, K. Slomkowski, "InP-based Negative Feedback Avalanche Diodes," *Proceedings of the SPIE* **7222**, 72221K (2009).
16. M.A. Itzler, R. Ben-Michael, C.-F. Hsu, K. Slomkowski, A. Tosi, S. Cova, F. Zappa and R. Ispasoiu, "Single photon avalanche diodes (SPADs) for 1.5 μ m photon counting applications", *J. Modern Optics* **54** (2-3), 283 – 304 (2007).
17. M.A. Itzler, X Jiang, R Ben-Michael, K Slomkowski, M.A. Krainak, S. Wu and X. Sun, "InGaAsP avalanche photodetectors for non-gated 1.06 μ m photon-counting receivers", *Proceedings of the SPIE* **6572**, 65720G (2007).
18. X. Jiang, M. A. Itzler, R. Ben-Michael, and K. Slomkowski, "InGaAsP–InP Avalanche Photodiodes for Single Photon Detection", *IEEE J. of Sel. Topics in Quantum Electronics* **13**(4), 895-905 (2007).
19. M.A. Itzler, X. Jiang, B.M. Onat and K. Slomkowski, "Progress in self-quenching InP-based single photon detectors", *Proceedings of the SPIE* **7608**, 760829 (2010).
20. X. Jiang, M. A. Itzler, B. Nyman, K. Slomkowski, "Negative Feedback Avalanche Diodes for Near-infrared Single Photon Detection," *Proceedings of the SPIE* **7320**, 732011 (2009).
21. M. M. Hayat, D.A. Ramirez, G.J. Rees and M.A. Itzler, "Modeling Negative Feedback in Single Photon Avalanche Diodes", *Proceedings of the SPIE* **7681**, 76810W (2010).
22. C.H. Tan, J.S. Ng, G.J. Rees and J.P.R. David, "Statistics of Avalanche Current Buildup time in Single Photon Avalanche Diodes", *IEEE J. of Selected Topics in Quantum Electronics* **13** (4), 906 (2007).
23. M.A. Ward and A. Vacheret, "Impact of after-pulse, pixel crosstalk and recovery time in multi-pixel photon counter response", *Nuclear Instruments and Methods in Physics Research A* **610**, 370 – 373 (2009).